

# Theory of superconductivity and mass enhancement near CDW critical point based on Bethe-Salpeter equation method: application to cuprates

Youchi Yamakawa\* and Hiroshi Kontani

*Department of Physics, Nagoya University, Nagoya 464-8602, Nagoya 464-8602, Japan*

(Dated: August 28, 2025)

In recent years, charge-channel orders in strongly correlated metals have attracted great attention. Famous examples are the electronic nematic orders in cuprates and iron-based superconductors, and Star-of-David order in kagome metals. Critical phenomena and unconventional superconductivity arising from fluctuations of such charge-channel orders are central issues today; however, the essential role is played by the vertex corrections, which are the many-body effects that are dropped in conventional mean-field type approximations. To solve this difficulty, in this study, we propose the Bethe-Salpeter equation theory to evaluate electron-electron interactions in two dimensional Hubbard models. This method satisfies the criteria of the Baym-Kadanoff conserving approximation. Here, we find that an attractive interaction in the charge channel emerges from the Aslamazov-Larkin vertex corrections that describe the interference processes among spin fluctuations. Applying this method to the square-lattice Hubbard model, we reveal that the cooperation of attractive charge fluctuations and repulsive spin fluctuations yields high- $T_c$   $d$ -wave superconductivity together with enhanced effective mass. These results naturally explain the phase diagram of cuprate superconductors, where strong-coupling  $d$ -wave superconductivity appears near the charge-order quantum critical point. The theory can also be applied to multi-orbital Hubbard models, like iron-based and nickelate superconductors, suggesting broad potential for future applications.

## I. INTRODUCTION

In recent years, many interesting quantum phases involving charge and orbital degrees of freedom have been discovered in strongly correlated metals. A representative example is the charge-density-wave (CDW) order in cuprate high- $T_c$  superconductors, which has been observed by  $X$ -ray scattering [1–9], scanning tunneling microscopy (STM) [10, 11], and nuclear magnetic resonance (NMR) [12–14]. In addition, the electronic nematic order in iron-based superconductors [15, 16], the  $2 \times 2$  CDW in kagome metals [17, 18], and loop-current order [19–21] have attracted considerable attention. These charge-channel orders arising from strong electron correlations do not necessarily accompany conventional spin-density-wave (SDW) order. In strongly correlated electron systems, the local Coulomb repulsion  $U$  is comparable to the bandwidth and promotes spin polarization, so conventional mean-field type approximations predict the pure SDW order. This fact strongly motivates researchers to improve previous theories of electronic correlations [4, 22].

Charge-channel orders in the above-mentioned strongly correlated metals are considered to be closely related to unconventional superconductivity. In  $d$ -wave cuprate superconductors, such as YBCO, both the superconducting transition temperature  $T_c$  and the upper critical field  $H_{c2}$  take their maximum values at the quantum critical point (QCP) at the end of the CDW phase for many cuprate compounds [3, 23, 24]. That is, strong-coupling superconductivity is realized at the

QCP of charge-channel order. Similar strong-coupling superconductivity is also observed at the end of the nematic order in the  $s$ -wave iron-based superconductor Fe(Se,Te) [25] and at the end of the  $2 \times 2$  CDW in the kagome-lattice superconductor CsV<sub>3</sub>Sb<sub>5</sub> [26]. To clarify such intriguing unconventional superconductivity in these systems, it is essential to use theoretical methods based on the Hubbard model that can correctly describe charge-channel orders and critical fluctuations.

In response to experimental progress, theoretical studies on the two-dimensional Hubbard model have also developed significantly in recent years. Research on  $d$ -wave superconductivity and spin/charge stripe orders has advanced through cluster dynamical mean-field theory (cDMFT) [27, 28], variational Monte Carlo (VMC) [29–31], and density-matrix renormalization group (DMRG) [32–34]. These theoretical methods can be applied even in the strong-coupling regime, although they suffer from finite-size effects. In addition, analyses based on field-theoretical approaches such as the functional renormalization group [35, 36] and the parquet renormalization group [37] have revealed that various charge-channel orders emerge due to many-body effects that are dropped in mean-field type approximations [38–43].

The authors have focused on the Aslamazov-Larkin (AL) type vertex correction, which describes the coupling between charge and spin fluctuations, and have explained the orbital order and nematic order in iron-based superconductors [44, 45], the CDW in cuprates [42, 46, 47], and the  $2 \times 2$  CDW in kagome metals [38]. The AL-type vertex correction describes magnon-pair formation in metals ( $\langle s_i s_j \rangle \neq 0$ ), under which a variety of charge-channel orders appear without spin order (i.e.,  $\langle s_i \rangle = 0$ ) [48]. This theory satisfies the criteria of the Baym-Kadanoff con-

---

\* yamakawa@s.phys.nagoya-u.ac.jp

serving approximation [49, 50], and it is applicable to various multi-orbital Hubbard models. The charge-channel orders produced by this mechanism correspond to modulations  $\delta t_{i,j}$  of the hopping integral, and are hereafter referred to as bond order (BO).

At the quantum critical point (QCP) at the end of an ordered phase in metals, well-developed quantum fluctuations of bosonic modes can give rise to unconventional superconductivity and quantum critical phenomena. The most extensively studied example is the QCP of the spin-density-wave (SDW) phase [51, 52]. The methods for calculating the interaction  $V_{\text{spin}}$  mediated by spin fluctuations have been developed in Refs. [53, 54]. In contrast, the theory for the QCP of the bond-order phase is still incomplete. The calculation methods for the interaction  $V_{\text{BO}}$  mediated by developed bond-order fluctuations have remained at a qualitative level. Once a method for calculating  $V_{\text{BO}}$  with high accuracy is established, one can to quantitatively study unconventional superconductivity and quantum critical phenomena mediated by bond-order fluctuations. Therefore, this theoretical problem is of great importance.

In this study, we propose the ‘‘Bethe-Salpeter (BS) equation theory’’ to quantitatively determine  $V_{\text{BO}}$ . This theory is based on the Baym-Kadanoff conserving approximation and systematically incorporates vertex corrections, such as the Maki-Thompson term and the Aslamazov-Larkin term. These vertex corrections describe the quantum interference among spin fluctuations. The  $V_{\text{BO}}$  obtained in this theory exhibits a pronounced momentum dependence and increases divergently near the QCP. We then apply the theory to the single-orbital square-lattice Hubbard model, which is an effective model for cuprate high- $T_c$  superconductors. As a result, we find that near the QCP of the  $d$ -wave bond order ( $p \sim 0.2$ ), spin fluctuations and bond-order fluctuations cooperate to realize the strong-coupling  $d$ -wave superconductivity (high  $T_c$  and  $H_{c2}$ ) and quantum critical phenomena (large  $m^*$ ) observed in experiments. This theory provides a clear physical understanding of the characteristic electronic state near the QCP in cuprate high- $T_c$  superconductors. We stress that the present theoretical framework can be easily applied to more complex multi-orbital metals, such as iron-based superconductors and Ni-based oxide superconductors.

## II. MODEL AND FLEX

First, we introduce the single-orbital Hubbard model and show the basic results of the fluctuation-exchange (FLEX) approximation, which will serve as the starting point for the BS equation discussed later. The Hamiltonian is

$$H = \sum_{\mathbf{k}, \sigma} \epsilon_{\mathbf{k}} c_{\mathbf{k}, \sigma}^\dagger c_{\mathbf{k}, \sigma} + U \sum_i n_{i, \uparrow} n_{i, \downarrow}, \quad (1)$$

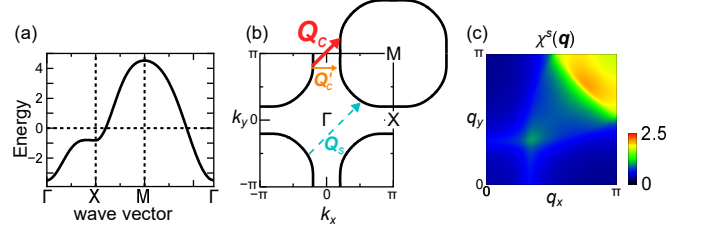


FIG. 1. (a) Band structure and (b) Fermi surface for hole doping  $p = 0.2$ . The nesting vector for spin fluctuations is  $\mathbf{Q}_s \approx (\pi, \pi)$ .  $\mathbf{Q}_c = (\delta, \delta)$  and  $\mathbf{Q}'_c = (\delta, 0)$  are the nesting vectors associated with charge-channel fluctuations; the experimentally observed CDW corresponds to  $\mathbf{Q}'_c$ . (c) Spin susceptibility  $\chi^s(\mathbf{q})$  calculated within FLEX for  $p = 0.2$ ,  $U = 4.29$ , and  $T = 0.01$ .

where  $c_{\mathbf{k}, \sigma}^\dagger$  creates an electron with wave vector  $\mathbf{k}$  and spin  $\sigma$ , and  $n_{i, \sigma} = c_{i, \sigma}^\dagger c_{i, \sigma}$  is the density operator.  $U$  is the local Coulomb interaction. The band dispersion is  $\epsilon_{\mathbf{k}} = -2t(\cos k_x + \cos k_y) - 4t' \cos k_x \cos k_y - 2t''(\cos 2k_x + \cos 2k_y)$ , and we use  $t = 1$ ,  $t' = -t/5$ , and  $t'' = t/6$  in this study.

Fermi surface and band structure for hole doping  $p = 0.2$  are shown in Figs. 1(a) and 1(b), respectively. The nesting vector of spin fluctuations is  $\mathbf{Q}_s \approx (\pi, \pi)$ , while candidate wave vectors for charge-channel fluctuations are  $\mathbf{Q}_c = (\delta, \delta)$  and  $\mathbf{Q}'_c = (\delta, 0)$ . The experimentally observed CDW corresponds to  $\mathbf{Q}'_c$ . Unless otherwise noted, we use the nearest-neighbor hopping  $|t| = 1$  ( $\sim 0.5$  eV) as the unit of energy.

Figure 1(c) presents the spin susceptibility calculated using FLEX,  $\chi^s(\mathbf{q}) = \frac{\chi^0(\mathbf{q})}{1 - \alpha_s(\mathbf{q})}$ , where  $\chi^0(\mathbf{q})$  is the irreducible susceptibility and  $\alpha_s(\mathbf{q}) \equiv U\chi^0(\mathbf{q})$  is the  $\mathbf{q}$ -dependent spin Stoner factor. The spin Stoner factor  $\alpha_s \equiv \max_{\mathbf{q}} [\alpha_s(\mathbf{q})]$  reaches unity at the SDW transition. For  $U = 4.29$ ,  $T = 0.01$ , and  $p = 0.2$ , we obtain  $\alpha_s = 0.9$ , indicating well-developed spin fluctuations around  $\mathbf{Q}_s$ .

In contrast, the charge susceptibility from FLEX,  $\chi^c(\mathbf{q}) = \frac{\chi^0(\mathbf{q})}{1 + \alpha_c(\mathbf{q})}$ ,  $\alpha_c(\mathbf{q}) \equiv -U\chi^0(\mathbf{q})$ , is strongly suppressed by  $U$ . This means that FLEX cannot reproduce charge-channel orders driven by local Coulomb repulsion.

## III. BETHE-SALPETER (BS) EQUATION

In this section, we introduce the Bethe-Salpeter (BS) equation formalism with full vertex corrections, which constitutes the central theoretical framework of this study.

### A. Formulation of the BS equation

By including the vertex corrections neglected in the FLEX [53], the Bethe-Salpeter (BS) equation provides a framework to describe the development of charge-channel

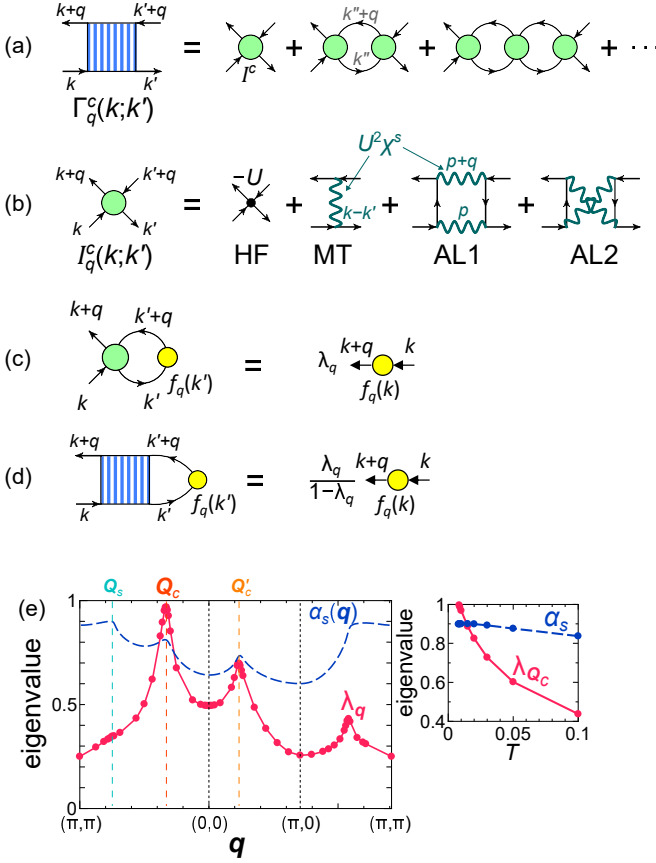


FIG. 2. (a) Diagrammatic representation of the Bethe-Salpeter (BS) equation for the full vertex  $\Gamma_q^c(k; k')$ .  $\Gamma_q$  increases as  $\propto I_q/(1 - \lambda_q)$  near the eigenvalue  $\lambda_q = 1$ , where  $\lambda_q$  corresponds to the instability in the charge channel, and  $1/(1 - \lambda_q)$  to the charge susceptibility. (b) Irreducible interaction  $I^c$ , consisting of one Hartree term, one Maki-Thompson (MT) term (first-order in fluctuations), and two Aslamazov-Larkin (AL) terms (second-order in fluctuations). (c) Density-wave (DW) equation with the form factor  $f_q(k)$  and eigenvalue  $\lambda_q$ ; the transition occurs at  $\lambda_q = 1$ . (d) Diagonalization equation for  $\Gamma$ , whose eigenvalue is  $\lambda_q/(1 - \lambda_q)$ , diverging at  $\lambda_q \rightarrow 1$  (particle-hole ordering transition). (e)  $q$ -dependence of  $\lambda_q$  and the spin Stoner factor  $\alpha_s(q)$  for  $p = 0.2$ ,  $U = 4.29$ , and  $T = 0.01$ .  $\lambda_q$  peaks at  $Q_c = (\delta, \delta)$  and  $Q'_c = (\delta, 0)$ , indicating the tendency toward charge-channel order with these wave vectors. Inset: Temperature dependence of  $\lambda_{Q_c}$  and  $\alpha_s$ , showing that  $\lambda_{Q_c}$  surpasses  $\alpha_s$  at low  $T$ , and the charge susceptibility diverges at  $T_{CDW} = 0.009$ .

fluctuations beyond mean-field theory. Within the microscopic Fermi-liquid theory [55], the BS equation for the full electron-electron vertex  $\Gamma_q^c(k, k')$  is given by

$$\Gamma_q^x(k, k') = I_q^x(k, k') - \frac{T}{N} \sum_{k''} I_q^x(k, k'') G(k'' + q) G(k'') \times \Gamma_q^x(k'', k'), \quad (2)$$

where  $x = c$  denotes the charge channel and  $x = s$  the spin channel. Here,  $k = (\mathbf{k}, i\epsilon_n)$  and  $q = (\mathbf{q}, i\omega_l)$  represent the combined notations for wave vector and Matsubara

frequency for fermions  $\epsilon_n = (2n + 1)\pi T$  and bosons  $\omega_l = 2l\pi T$ . Solving Eq. (2) self-consistently yields the full charge-channel vertex  $\Gamma_q^c(k, k')$  [Fig. 2(a)].

The vertex corrections are included in the irreducible interaction  $I_q^c(k, k')$  in the particle-hole (p-h) channel [Fig. 2(b)], which is derived from the one-loop approximation of the Luttinger-Ward functional  $\Phi^{LW}$  [50]. It consists of the Hartree term ( $U$ ), the Maki-Thompson (MT) term, and two Aslamazov-Larkin (AL) terms. The explicit expressions for  $I^c$  and  $I^s$  are given in Appendix A. If only the Hartree term is retained, the susceptibilities of the FLEX approximation are reproduced. The MT and AL terms represent vertex corrections that describe correlations beyond FLEX. In particular, the AL terms drive the CDW instability via quantum interference between SDW fluctuations, and successfully explain the nonmagnetic nematic order in FeSe [45] and the CDW in CsV<sub>3</sub>Sb<sub>5</sub> [38]. The importance of the MT and AL terms has also been confirmed using unbiased many-body methods such as the functional renormalization group [39–42].

The superconducting (SC) gap equation is equivalent to the BS equation in the particle-particle (p-p) channel, where it is well established that the MT term drives unconventional SC states with sign-reversals [56]. Recently, the importance of the MT and AL terms in the particle-hole channel BS equation has been discovered as explained in Ref. [48].

## B. Physical interpretation of $\Gamma_q(k, k')$

To understand the  $q$ ,  $k$ , and  $k'$  dependences of  $\Gamma_q^c(k, k')$ , we consider the density-wave (DW) equation shown in Fig. 2(c) [50]. Here,  $f_q(k)$  is the form factor describing the nonlocal structure of the DW order, and  $\lambda_q$  is its largest eigenvalue characterizing the instability; the DW transition temperature is given by  $\lambda_q = 1$ . Replacing the kernel  $I^c$  in the DW equation with the full vertex  $\Gamma^c$  yields eigenvalues of  $f_q(k)$  as  $\lambda_q/(1 - \lambda_q)$  [Fig. 2(d)]. Thus, for  $\lambda_q \approx 1$ ,  $\Gamma_q^c$  is well approximated by

$$\Gamma_q^c(k, k') \approx f_q(k) \frac{\bar{I}_q^c}{1 - \lambda_q} f_q^*(k'), \quad (3)$$

which increases critically near  $q \approx Q_c$ . (Mathematically, Eq. (3) corresponds to the maximum eigenvalue component in a singular value decomposition.) The proportional relation  $\Gamma_q^c \propto \bar{I}_q^c/(1 - \lambda_q) \propto \lambda_q/(1 - \lambda_q)$  in Eq. (3) holds exactly only when  $\Gamma^c$  is obtained by solving the BS equation without approximation, that is, with full summations over all internal  $\mathbf{k}$  and  $\epsilon_n$ .

Once  $\Gamma_q(k, k')$  is accurately determined, various physical quantities, such as the superconducting gap function and the self-energy, can be calculated. While Eq. (3) corresponds to the leading term in a singular-value decomposition and is quantitatively reliable only near the QCP, in this study we solve the BS equation numerically

in two dimensions to obtain  $\Gamma^c$  with high precision for all  $q$ ,  $k$ , and  $k'$ , irrespective of the distance from the QCP. (The  $\Gamma^c$  obtained from the BS equation naturally satisfies Eq. (3) near the QCP.) This “BS equation theory” thus enables quantitative calculations of critical phenomena across a wide range of physical quantities.

Figure 2(e) shows the  $q$ -dependence of  $\lambda_q$  for  $U = 4.29$ ,  $T = 0.01$ , and  $p = 0.2$ .  $\lambda_q$  exhibits peaks at  $\mathbf{Q}_c$  and  $\mathbf{Q}'_c$ , indicating the stabilization of charge-channel orders (such as CDW or bond order) with these wave vectors. The inset plots the temperature dependence of  $\lambda_{\mathbf{Q}_c}$  and the spin Stoner factor  $\alpha_s$ . As the temperature decreases,  $\lambda_{\mathbf{Q}_c}$  overtakes  $\alpha_s$ , and the charge susceptibility  $\propto 1/(1 - \lambda_{\mathbf{Q}_c})$  increases divergently toward the critical temperature  $T_{\text{CDW}} = 0.009$ .

### C. Numerical results for vertex functions

In this subsection, we denote the four-point vertex as

$$\Gamma^x(k_1, k_2; k_3, k_4) \quad (4)$$

Here,  $k_1$  and  $k_4$  are outgoing, while  $k_2$  and  $k_3$  are incoming. Equation (4) corresponds to  $\Gamma_q^x(k_2, k_4) \delta_{k_1 - k_2, q}$  ( $q = k_3 - k_4$ ) in Eq. (2). Here we introduce the p-h and p-p channel vertices to discuss the self-energy correction and the pairing instability,

$$\Gamma_{ph}^x(k, k') \equiv \Gamma^x(k', k; k', k), \quad (5)$$

$$\Gamma_{pp}^x(k, k') \equiv \Gamma^x(k, k'; -k', -k). \quad (6)$$

Figures 3(a) and 3(b) show  $\Gamma_{ph}^c(\theta, \theta')$  and  $\Gamma_{pp}^c(\theta, \theta')$  obtained from the BS equation for  $U = 4.29$ ,  $T = 0.01$ , and  $p = 0.2$ , with  $\mathbf{k}$  and  $\mathbf{k}'$  restricted to the Fermi surface [Fig. 3(c)] and  $\epsilon_n = \epsilon_{n'} = \pi T$ . In both channels,  $\Gamma^c$  is strongly enhanced for  $(\theta, \theta')$  satisfying  $\mathbf{k}_\theta - \mathbf{k}_{\theta'} \approx \mathbf{Q}_c$ , in agreement with the Eq. (3). This indicates the development of an effective interaction mediated by bond-order fluctuations. The nesting geometry is illustrated in Fig. 3(d), which will be shown in the next section to account for the enhancement of the effective mass and d-wave pairing near the CDW QCP.

Figure 3(e) shows the  $U$  dependence of  $I^c = (I_{ph}^c + I_{pp}^c)/2$  averaged along the dashed line in Fig. 3(a). In the weak-coupling regime  $U \ll N(0)^{-1}$ , the RPA relation  $I^c = -U$  holds. As  $U$  increases, vertex corrections, especially the AL terms, make  $I^c$  positive and even  $I^c \gg U$  [38, 39, 57–60]. Consequently,  $\Gamma^c$  given by Eq. (3) becomes crucial near the CDW QCP.

The  $U$  dependence of the normalized full vertex  $(1 - \lambda_{\mathbf{Q}_c})\Gamma_{ph}^c/U$  is plotted in Fig. 3(f), showing a close similarity to  $I^c/U$ . Figure 3(g) further demonstrates that  $\Gamma^c$  scales as  $\lambda_{\mathbf{Q}_c}/(1 - \lambda_{\mathbf{Q}_c})$  for  $\lambda_{\mathbf{Q}_c} \lesssim 1$ , confirming the validity of Eq. (3).

We note that  $\Gamma^c$  obtained from the BS equation is strongly enhanced near  $\lambda_{\mathbf{Q}_c} \approx 1$  only in the low-frequency region. Therefore, in the present numerical

study, we employ a lowest-Matsubara-frequency approximation, where  $\Gamma^c$  at  $|\epsilon_n| = \pi T$  is computed from the BS equation including vertex corrections. This approximation is justified near the QCP, where the energy scale of CDW fluctuations is small, and it provides a lower-bound estimate of vertex-correction effects.

### IV. MASS ENHANCEMENT

Using the  $\Gamma^c$  obtained by solving the BS equation in the previous section, we now evaluate the enhancement of the quasiparticle effective mass. In strongly correlated electron systems, the effective mass  $m^*$  is significantly increased, strongly influencing many physical properties such as the specific heat and superconductivity.

Figure 4(a) shows the Ward identity for the mass-enhancement factor  $Z = m^*/m$ :

$$Z(\mathbf{k}) = 1 - \left. \frac{\partial}{i\partial\omega} \Sigma(\mathbf{k}, i\omega) \right|_{\omega=0}. \quad (7)$$

Here, the solid line with a slash represents  $\left. \frac{\partial}{i\partial\omega} G(\mathbf{k}, i\omega) \right|_{\omega=0}$ . The vertex  $\Gamma$  corresponds to the four-point vertex given in Eq. (2), which includes interactions beyond the Migdal approximation (FLEX). A more detailed explanation is provided in Appendix B.

The angular dependence of  $Z(\theta)$  along the Fermi surface for  $U = 4.29$ ,  $T = 0.01$ , and  $p = 0.2$  is shown in Fig. 4(b). Here we compare the results obtained by BS with those obtained by FLEX ( $Z_{\text{FLEX}}$ ). When the CDW fluctuations are weak,  $Z(\theta) \gtrsim Z_{\text{FLEX}}(\theta)$ . In contrast, when the CDW fluctuations are strong,  $Z(\theta) \gg Z_{\text{FLEX}}(\theta)$  around the hot spots. Figure 4(c) presents a color plot of  $Z(\theta)$  obtained by the BS equation. In the BS equation theory, the remarkable enhancement of  $\Gamma_{ph}^c(\theta, \theta')$  around  $\mathbf{k} - \mathbf{k}' \sim \mathbf{Q}_c$  [see Fig. 3(a)] leads to strong mass enhancement at the hot spots. In FLEX, by contrast, the angular dependence of  $Z(\theta)$  remains relatively weak [54, 61].

Furthermore, Fig. 4(d) shows the temperature dependence of the electronic specific-heat coefficient,  $\gamma = \frac{1}{N} \sum_{\mathbf{k}} Z_{\mathbf{k}} \rho_{\mathbf{k}}$ , where  $\rho_{\mathbf{k}} = \delta(\mu - \epsilon_{\mathbf{k}})$ . Note that the specific heat coefficient of the electron gas is given by  $\gamma_0 = (1/N) \sum_{\mathbf{k}} \rho_{\mathbf{k}}$ . The BS result shows that  $\gamma$  is enhanced compared to FLEX due to charge-channel fluctuations.

Near the CDW-QCP, at low temperatures ( $T < 0.01$ ), quantum critical effects beyond the lowest-Matsubara-frequency approximation are expected to give rise to a  $\log T$  dependence [56, 62]. This issue is left as a future problem.

### V. SUPERCONDUCTIVITY

In this section, we analyze the superconducting state by solving the linearized gap equation using the interaction  $\Gamma$  obtained from the BS equation.



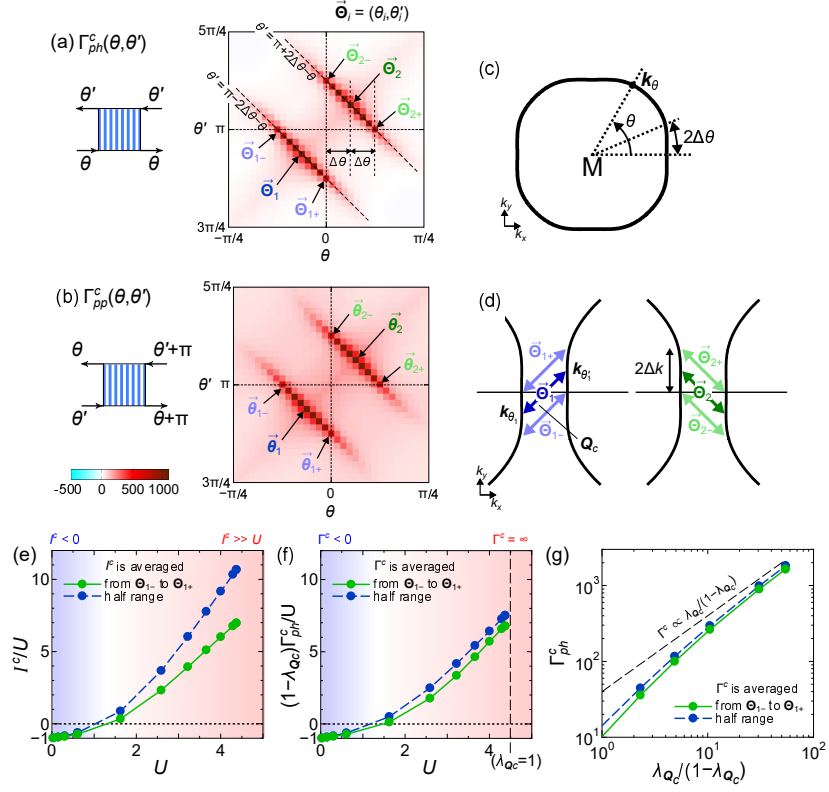


FIG. 3. (a) Particle-hole (p-h) channel vertex  $\Gamma_{ph}^c(\theta, \theta')$  and (b) particle-particle (p-p) channel vertex  $\Gamma_{pp}^c(\theta, \theta')$  obtained from the BS equation for  $U = 4.29$ ,  $T = 0.01$ , and  $p = 0.2$ . Both  $\Gamma_{ph}^c$  and  $\Gamma_{pp}^c$  are strongly enhanced and positive near the points  $\Theta_{1,2} = (\theta_{1,2}, \theta'_{1,2})$ , where  $\theta$  denotes the FS angle shown in (c) and  $\epsilon_n = \epsilon_{n'} = \pi T$ . (c) Fermi surface and definition of  $\theta$ . (d) Schematic illustration of the nesting condition: between  $\Theta_{1-}$  and  $\Theta_{1+}$  and between  $\Theta_{2-}$  and  $\Theta_{2+}$ , the relation  $\mathbf{k}_\theta - \mathbf{k}_{\theta'} \approx \mathbf{Q}_c$  is satisfied, giving strong  $\Gamma$  over a range  $\pm 2\Delta k \sim \pm 2k_F \Delta\theta$ . (e)  $U$  dependence of the normalized irreducible interaction  $I^c/U$  averaged along the dashed line in (a), where  $I^c = \frac{1}{2}(I_{ph}^c + I_{pp}^c)$ . (f)  $U$  dependence of the normalized full vertex  $(1 - \lambda_{Qc})\Gamma_{ph}^c/U$ , consistent with  $\Gamma^c \approx I^c/(1 - \lambda_{Qc})$ . The same holds for  $\Gamma_{pp}^c$ . (g)  $\Gamma_{ph}^c$  as a function of  $\lambda_{Qc}/(1 - \lambda_{Qc})$ , showing proportionality for  $\lambda_{Qc} \lesssim 1$ .

In the conventional Migdal approximation, the electron-fluctuation coupling constant  $U$  is fixed. In contrast, we previously introduced the  $U$ -VC theory to go beyond the Migdal approximation. There, the coupling constant between charge-channel fluctuations and Cooper pairs is significantly enhanced to  $U\Lambda^c$  due to the AL-type vertex correction  $\Lambda^c (\gg 1)$  [39, 57–60, 63, 64]. In the present BS theory, as shown in Fig. 3(d), the irreducible vertex  $I^c$  is strongly enhanced by the AL-type vertex correction, consistently with the previous studies. The diagrammatic representation of the gap equation using  $\Gamma$  is shown in Fig. 5(a). Superconductivity emerges when the eigenvalue  $\lambda_{SC}$  reaches unity. Here, the self-energy from FLEX is used for the Green's function, and the lowest-Matsubara-frequency approximation is applied to  $\Gamma$  (see Appendix C).

Based on the Fermi-liquid theory, the observed SC gap is  $\Delta(\theta) = \bar{\Delta}(\theta)/Z(\theta)$ . Here,  $\bar{\Delta}$  is the solution of the SC gap equation, Eq. (C4). The angular dependence of  $\Delta(\theta)$  is shown in Fig. 5(b). It is found that the attractive contribution from  $\Gamma^c$  is partially suppressed by mass renormalization, resulting in a  $d$ -wave superconducting gap

similar to that obtained by FLEX (within the Migdal approximation).

Figure 5(c) illustrates that spin and charge fluctuations act at different wave vectors and cooperatively stabilize  $d$ -wave superconductivity. While the spin channel provides repulsion near  $\mathbf{Q}_s$ , the charge channel supplies attraction near  $\mathbf{Q}_c$ , thereby naturally explaining strong-coupling  $d$ -wave superconductivity near the CDW-QCP.

The  $U$ -dependence of the eigenvalue  $\lambda_{SC}$  is presented in Fig. 5(d). Compared with the spin-fluctuation theory based on FLEX, the BS equation theory shows a pronounced enhancement of  $\lambda_{SC}$  and the transition temperature  $\bar{T}_{SC}$  ( $\bar{T}_{SC}$  is the temperature at which the eigenvalue  $\lambda_{SC}$  of the gap equation [Eq. (C4)] reaches unity.) due to the bond-order fluctuation interaction  $V_{BO}$ . Importantly, the attractive interaction from BO fluctuations is comparable in magnitude to the repulsive interaction from spin fluctuations, and both channels cooperate to realize high- $T_c$   $d$ -wave superconductivity.

According to Fermi-liquid theory, the superconducting transition temperature is renormalized by  $Z^{-1}$ . In the present calculation, the Green's functions  $G(\pm p)$  in

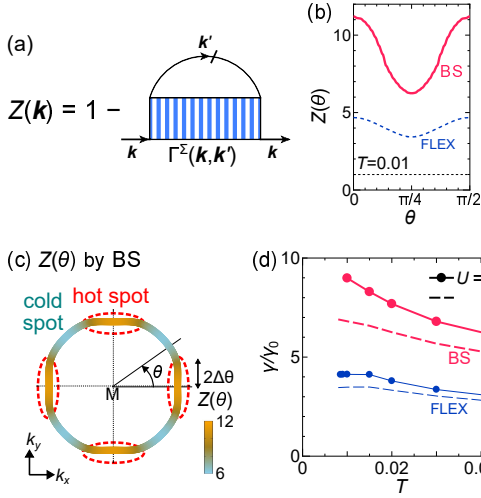


FIG. 4. (a) Diagram of the mass-enhancement factor  $Z(\mathbf{k})$  using  $\Gamma^\Sigma$ . The solid line with a slash represents  $\frac{\partial G(\mathbf{k})}{i\partial\omega}$ . The precise definition of  $\Gamma^\Sigma$  is given in Appendix B. (b)  $Z(\theta)$  obtained by BS (red solid line) and  $Z_{\text{FLEX}}(\theta)$  obtained by FLEX (blue dashed line) for  $p = 0.2$ ,  $U = 4.29$ , and various  $T$ . (c) Color plot of  $Z(\theta)$  obtained by BS. Due to the strong peak in  $\Gamma_{ph}^c$  originating from bond-order (BO) fluctuations,  $Z(\theta)$  is significantly enhanced within the angular range  $2\Delta\theta$ . (d) Temperature dependence of the enhancement of the electronic specific-heat coefficient  $\gamma/\gamma_0$  obtained by BS for  $U = 4.0$  and  $4.29$  with  $p = 0.2$ . The result  $\gamma_{\text{FLEX}}/\gamma_0$  obtained by FLEX is also shown.

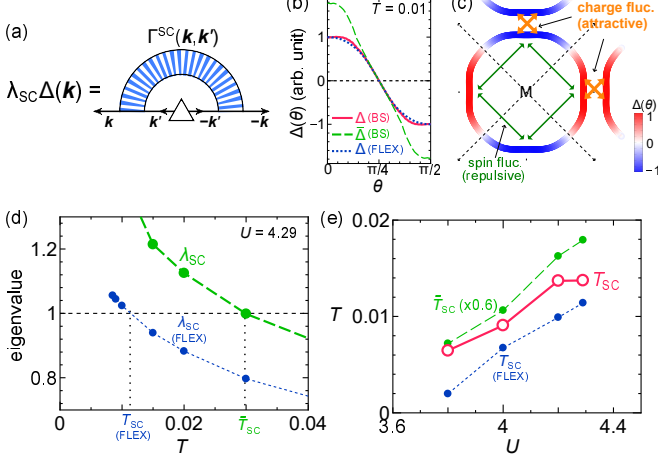


FIG. 5. (a) Diagram of the linearized gap equation using  $\Gamma$ . (b) Angular dependence of the gap functions  $\Delta$  and  $\bar{\Delta}$  by BS for  $U = 4.29$ ,  $T = 0.01$ , and  $p = 0.2$ , where the renormalized gap function is  $\Delta(\theta) = \bar{\Delta}(\theta)/Z(\theta)$ . The result of FLEX is also shown. The magnitude of  $\Delta$  is normalized by the slope at  $\theta = \pi/4$ . (c)  $d$ -wave superconducting structure mediated by spin and charge fluctuations. (d)  $U$ -dependence of  $\lambda_{\text{SC}}$ . (e)  $U$ -dependence of  $T_{\text{SC}}$  and  $\bar{T}_{\text{SC}}$ , where  $T_{\text{SC}} = \bar{T}_{\text{SC}} \cdot (\gamma_{\text{FLEX}}/\gamma)$ .

the gap equation [Eq. (C4)] include the factor  $Z_{\text{FLEX}}^{-1}$ . Thus, the superconducting transition temperature renormalized by the total mass-enhancement factor  $Z$ , which

is shown in 4, is given by

$$T_{\text{SC}} = \bar{T}_{\text{SC}} \cdot \frac{Z_{\text{FLEX}}}{Z}. \quad (8)$$

Note that  $\frac{Z_{\text{FLEX}}}{Z} = \frac{\gamma_{\text{FLEX}}}{\gamma}$ . Figure 5(e) shows the  $U$  dependence of  $\bar{T}_{\text{SC}}$ ,  $T_{\text{SC}}$ , and  $T_{\text{SC}}^{\text{FLEX}}$  from Migdal theory. Here,  $\gamma$  is evaluated at  $T = 0.01$ . Although  $\bar{T}_{\text{SC}} \sim 3T_{\text{SC}}^{\text{FLEX}}$ , the inclusion of BO-induced renormalization reduces it to  $T_{\text{SC}} \gtrsim T_{\text{SC}}^{\text{FLEX}}$ .

In summary, strong-coupling  $d$ -wave high- $T_c$  superconductivity emerges from the cooperative action of spin and charge channels.

## VI. PHASE DIAGRAM

Figure 6(a) shows the phase diagram obtained from the BS equation for  $U = 4$ . We plot the  $p$ -dependence of  $T_{\text{CDW}}$  obtained from the DW equation and  $T_{\text{SC}}$  obtained from Eq. (8). Here,  $T_{\text{CDW}}$  is a monotonically decreasing function of  $p$ , whereas  $T_{\text{SC}}$  exhibits a gentle peak around  $p \sim 0.18$ . Moreover, the relation  $T_{\text{CDW}} \sim T_{\text{SC}}$  at  $p \sim 0.15$ , and  $T_{\text{CDW}} < T_{\text{SC}}$  holds for  $p > 0.15$ . These results are consistent with experiments [22]. In Fig. 6(a), in addition to  $T_{\text{CDW}}$  ( $\lambda = 1$ ), we also show the  $p$ -dependence for  $\lambda = 0.98, 0.95$ , and  $0.90$ . In regions where CDW fluctuations are well developed, nanoscale CDW domains may emerge around a small amount of impurities and can give rise to a pseudogap. Figure 6(b) shows the phase diagram for  $U = 4.29$ , where  $T_{\text{SC}}$  is enhanced. The obtained value of  $T_{\text{SC}} \sim 0.01|t|$  ( $\sim 50$  K) corresponds to that of the single-layer cuprate LSCO. It should be noted that the competition between superconductivity and CDW leads to the suppression of  $T_{\text{CDW}}$  within the superconducting phase and vice versa.

The doping dependence of the orbital upper critical field  $H_{c2}$  is shown in Figure 6(c). It is estimated from  $H_{c2} = \phi_0/(2\pi\xi_{\text{GL}}^2)$  with  $\xi_{\text{GL}} = \hbar v_F/(\pi\Delta_0)$ , giving  $H_{c2} \propto (T_c\gamma/\gamma_0)^2$ . Here,  $\gamma$  at  $T = 0.01$  is used. Within the BS theory including charge-channel interactions, both  $H_{c2}$  and  $\gamma$  are strongly enhanced compared with FLEX.

A schematic phase diagram is shown in Fig. 6(d). Near the CDW quantum critical point, a pseudogap region emerges due to short-range CDW correlations, and a  $d$ -wave high- $T_c$  superconducting phase is realized through the cooperative effects of BO and spin fluctuations.

## VII. DISCUSSIONS AND CONCLUSIONS

We have developed a Bethe-Salpeter (BS) theory that enables a quantitative evaluation of the effective interaction  $V_{\text{BO}}$  beyond the mean-field approximation. This theory, systematically includes vertex corrections such as the Maki-Thompson and Aslamazov-Larkin terms. As a result, it provides a non-empirical way to derive attractive interactions mediated by fluctuations. The calcu-

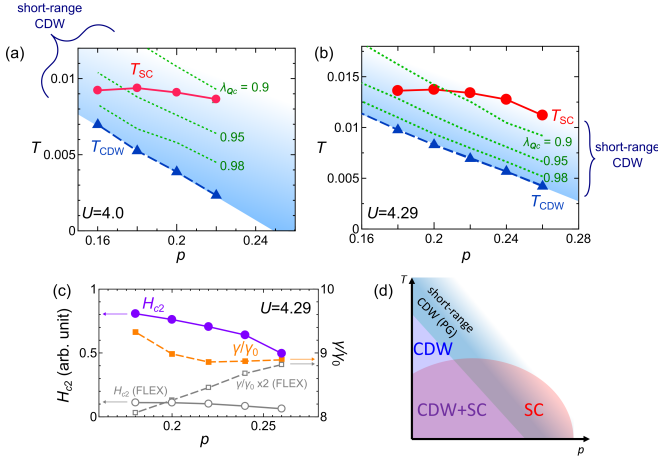


FIG. 6. (a)(b) Doping dependence of the transition temperatures obtained from the present theory for (a)  $U = 4$  and (b)  $U = 4.29$ . The blue dashed line with triangles represents  $T_{CDW}$  determined from  $\lambda_{Qc} = 1$ , while the red solid line with circles denotes  $T_{SC}$ . The green dashed lines correspond to  $\lambda_{Qc} = 0.98, 0.95, 0.90$ . (c) Doping dependence of  $H_{c2} \propto (T_c \gamma / \gamma_0)^2$  and  $\gamma / \gamma_0$  at  $U = 4.29$ . Within the BS theory, both  $H_{c2}$  and  $\gamma$  are strongly enhanced compared to those obtained by FLEX, owing to the development of BO fluctuations. (d) Schematic phase diagram, where  $T_{SC}$  is enhanced in the vicinity of the CDW phase.

lated  $V_{BO}$  shows strong momentum dependence and diverges near the bond-order (BO) quantum critical point (QCP).

By applying this method to the single-band Hubbard model, we showed that spin and BO fluctuations cooperate to produce strong-coupling  $d$ -wave superconductivity near the BO QCP ( $p \sim 0.2$ ). In this region, both the superconducting transition temperature  $T_c$  and the upper critical field  $H_{c2}$  are strongly enhanced, accompanied by a large increase in the effective mass  $m^*$ . These results give a consistent microscopic picture of superconductivity and quantum criticality in cuprates. The possible effects of bilayer Fermi-surface splitting [65] would be an interesting future issue.

The enhancement of  $V_{BO}$  by vertex corrections agrees with previous theoretical studies [38, 57, 58, 66]. The BS equation theory can also be applied to multiorbital systems. Indeed, it has recently been used to study nickelates [67], and its application to iron-based superconductors, where nematic and smectic fluctuations are important, would be fruitful.

In the present numerical study, we employed the lowest-Matsubara-frequency approximation for  $\Gamma_q(k, k')$  with respect to  $q, k$ , and  $k'$ , while fully summing over internal Matsubara frequencies. In the BS equation theory, however, calculations for arbitrary external Matsubara frequencies are possible. Such an extension would allow quantitative studies at lower temperatures, and remains an important future task.

## ACKNOWLEDGMENTS

The authors are grateful to Rina Tazai and Seiichiro Onari for fruitful discussions. This work was supported by JSPS KAKENHI (Grant Numbers JP20K03858, JP24K00568, and JP24K06938).

## Appendix A: Formulation of the Bethe-Salpeter Equation

In this study, we introduce the Bethe-Salpeter (BS) equation, which plays a central role, and determine the four-point vertex  $\Gamma$  representing the full interaction. The BS equation is given by the following self-consistent form:

$$\begin{aligned} \Gamma_q^{\sigma\sigma'\sigma''\sigma'''}(k, k') &= I_q^{\sigma\sigma'\sigma''\sigma'''}(k, k') \\ &+ \frac{T}{N} \sum_{k''} \sum_{\rho\rho'\rho''\rho'''} I_q^{\sigma\sigma'\rho\rho'}(k, k'') G^{\rho\rho''}(k'' + q) G^{\rho'''\rho'}(k'') \\ &\times \Gamma_q^{\rho''\rho'''\sigma''\sigma'''}(k'', k) \end{aligned} \quad (A1)$$

Here,  $k = (\mathbf{k}, i\epsilon_n)$  and  $q = (\mathbf{q}, i\omega_l)$  denote combined notations for momentum and Matsubara frequencies for fermion  $\epsilon_n = (2n + 1)\pi T$  and boson  $\omega_l = 2l\pi T$ , respectively.  $\sigma, \rho = \uparrow, \downarrow$  denote the spin indices at each vertex, as illustrated in Fig. 7.  $I$  is the irreducible vertex, whose explicit form will be given later. Assuming that the system satisfies SU(2) symmetry, the spin dependence of  $\Gamma$  can be expressed in terms of the charge-channel vertex  $\Gamma^c$  and the spin-channel vertex  $\Gamma^s$  as

$$\begin{aligned} \Gamma_q^{\sigma\sigma'\sigma''\sigma'''}(k, k'') &= \Gamma_q^c(k, k'') \delta_{\sigma, \sigma'} \delta_{\sigma'', \sigma'''} \\ &+ \Gamma_q^s(k, k'') \boldsymbol{\sigma}_{\sigma, \sigma'} \cdot \boldsymbol{\sigma}_{\sigma'', \sigma'''} \end{aligned} \quad (A2)$$

where  $\boldsymbol{\sigma}$  represents the Pauli matrices.

Under SU(2) symmetry, the Green's function is  $G^{\sigma\sigma'}(k) = G(k) \delta_{\sigma\sigma'}$ , and the BS equation is separated into the charge channel ( $x = c$ ) and spin channel ( $x = s$ ) as

$$\begin{aligned} \Gamma_q^x(k, k') &= I_q^x(k, k') \\ &- \frac{T}{N} \sum_{k''} I_q^x(k, k'') G(k'' + q) G(k'') \Gamma_q^x(k'', k') \end{aligned} \quad (A3)$$

From Eq. (A2), the charge (spin) channel vertices  $X^{c(s)} = \Gamma^{c(s)}, I^{c(s)}$  are given by

$$X^c = X^{\uparrow\uparrow\uparrow\uparrow} + X^{\uparrow\uparrow\downarrow\downarrow} \quad (A4)$$

$$X^s = X^{\uparrow\uparrow\uparrow\uparrow} - X^{\uparrow\uparrow\downarrow\downarrow} = X^{\uparrow\downarrow\uparrow\downarrow} \quad (A5)$$

The irreducible vertex  $I$  appearing in Eq. (A1) is defined as the functional derivative of the Luttinger-Ward functional  $\Phi^{LW}$ . For example, in the case of  $q = 0$ , it is expressed as

$$I_0^{\sigma\sigma'\sigma''\sigma'''}(k, k') = \frac{\delta^2 \Phi^{LW}[G]}{\delta G_k^{\sigma'\sigma} \delta G_{k'}^{\sigma''\sigma'''}} \quad (A6)$$

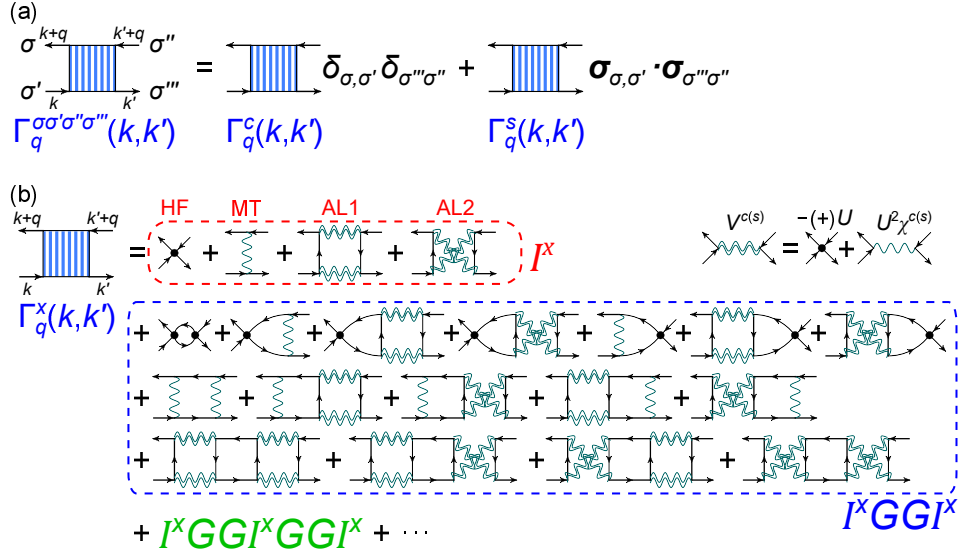


FIG. 7. (a) The full four-point vertex  $\Gamma_q^{\sigma\sigma'\sigma''\sigma'''}(k, k')$ . Under SU(2) symmetry, it is represented by  $\Gamma^c$  and  $\Gamma^s$ . (b) Diagrammatic expression of  $\Gamma$  obtained by solving the BS equation. The double wavy line denotes  $V^{c(s)} = -(+)U + U^2\chi^{c(s)}$ .

In this study, we adopt the one-loop approximation for  $\Phi^{\text{LW}}$ , which decomposes into the following four terms:

$$I^x = I^{\text{HF},x} + I^{\text{MT},x} + I^{\text{AL1},x} + I^{\text{AL2},x} \quad (\text{A7})$$

The Hartree-Fock (HF) term (Hartree term in the single-orbital case) is simply

$$I_q^{\text{HF},c}(k, k') = I^{\text{HF},c} = -U \quad (\text{A8})$$

$$I_q^{\text{HF},s}(k, k') = I^{\text{HF},s} = U \quad (\text{A9})$$

The Maki-Thompson (MT) term corresponds to the one-magnon exchange process in the spin and charge channels, and is given by

$$I_q^{\text{MT},c}(k, k') = -\frac{1}{2}V^c(k - k') - \frac{3}{2}V^s(k - k') + U + U^2\chi^0(k - k') \quad (\text{A10})$$

$$I_q^{\text{MT},s}(k, k') = -\frac{1}{2}V^c(k - k') + \frac{1}{2}V^s(k - k') - U \quad (\text{A11})$$

Here,  $V^{c(s)}(q) = \pm U + U^2\chi^{c(s)}(q)$  denotes the effective interaction in the charge (spin) channel obtained within FLEX. The terms  $U$  and  $U^2\chi^0$  serve as corrections for double counting with the HF term and the AL1 term, respectively. The Aslamazov-Larkin (AL) terms correspond to two-magnon processes describing interference of spin fluctuations:

$$I_q^{\text{AL1},x}(k, k') = \frac{T}{N} \sum_{q'} W^{x,1}(q, q') G(k - q') G(k' - q') \quad (\text{A12})$$

$$I_q^{\text{AL2},x}(k, k') = \frac{T}{N} \sum_{q'} W^{x,2}(q, q') G(k + q + q') G(k' - q') \quad (\text{A13})$$

The functions  $W^{x,n}(q, q')$  represent convolution terms of the spin and charge channels, given by

$$W^{c,n}(q, q') = \frac{1}{2}V^c(q - q')V^c(q') + \frac{3}{2}V^s(q - q')V^s(q') - U^2 \quad (\text{A14})$$

$$W^{s,n}(q, q') = \frac{1}{2}V^c(q - q')V^s(q') + \frac{1}{2}V^s(q - q')V^c(q') - (-1)^n V^s(q - q')V^s(q') \quad (\text{A15})$$

Here again, the term  $-U^2$  is a correction for double counting.

The diagrammatic structures incorporated by solving the BS equation are shown in Fig. 7(b). In RPA and FLEX approximations, the irreducible vertex  $I$  is approximated only by the Hartree term, which leads to  $\Gamma^x = V^x$ . In contrast, the higher-order terms beyond  $V^x$  originate from vertex corrections, and they are automatically incorporated within the BS equation theory.

Since  $\chi^s$  is strongly enhanced within FLEX, the most significant contributions in the charge channel term of Eq. (A14) are the AL1 and AL2 terms. These describe the interference effects of two paramagnons via  $W^c \propto V^s V^s$ , which strongly enhance charge fluctuations [48].

On the other hand, in Eq. (A15), the  $\pm V^s V^s$  terms included in  $W^s$  are small for even-parity spin fluctuations. For ordinary spin fluctuations, the AL1 and AL2 terms largely cancel each other. The  $V^c V^s$  terms are small, and hence vertex corrections in the spin channel are weak [39, 59]. Nevertheless, the  $V^s V^s$  terms in Eq. (A15) may potentially give rise to odd-parity orders such as spin-loop currents [68].

The present theory, when combined with the one-loop self-energy  $\Sigma_{\text{FLEX}}$  from FLEX, satisfies the Baym-Kadanoff conservation laws (particle number, energy, and momentum conservation).



## Appendix B: Mass enhancement factor using $\Gamma$

First, within Fermi-liquid theory, the exact expression for the mass enhancement factor  $Z$  is given by [55]

$$Z(k) = 1 - \frac{\partial \Sigma(k)}{i\partial\omega} = 1 - \frac{T}{N} \sum_p \tilde{I}^{ph}(k, p) \frac{\partial G(p)}{i\partial\omega}, \quad (\text{B1})$$

where  $\tilde{I}^{ph}$  denotes the exact particle-hole irreducible four-point vertex. The diagrammatic expression of  $Z$  is shown in Fig. 8(a).

Next, within the BS equation theory,  $\tilde{I}^{ph}$  is approximated as

$$\tilde{I}^{ph}(k, p) = \Gamma^\Sigma(k, p), \quad (\text{B2})$$

and

$$\Gamma^\Sigma(k, p) = \frac{1}{2} \Gamma_{ph}^c(k, p) + \frac{3}{2} \Gamma_{ph}^s(k, p), \quad (\text{B3})$$

which is shown in Fig. 8(b). In Fig. 8(b), the double counting terms that should be subtracted are expressed.

Finally, in the present numerical calculation,

$$Z(\mathbf{k}) = 1 - \frac{T}{N} \sum_{\mathbf{p}} \Gamma^\Sigma(\mathbf{k}, \mathbf{p}) \rho_{\mathbf{p}}. \quad (\text{B4})$$

Here,  $\Gamma^\Sigma(\mathbf{k}, \mathbf{p})$  is the lowest-Matsubara-frequency approximation. Also,  $\Gamma_{ph}^s$  is taken from FLEX (i.e.,  $\Gamma_{ph}^s = V^s$ ).

As an indicator of the effective mass enhancement, we also consider the electronic specific heat coefficient  $\gamma$ , which is given by the expectation value of  $Z(\mathbf{k})$  on the Fermi surface:

$$\gamma = \frac{1}{N} \sum_{\mathbf{k}} Z(\mathbf{k}) \rho_{\mathbf{k}}. \quad (\text{B5})$$

Defining  $\gamma_0$  as the specific heat coefficient without renormalization, the momentum-averaged mass enhancement factor is expressed as  $Z \equiv \gamma/\gamma_0$ .

## Appendix C: Linearized gap equation using $\Gamma$

First, within Fermi-liquid theory, the exact expression for the linearized gap equation is [55]

$$\lambda_{\text{SC}} \bar{\Delta}(k) = \frac{T}{N} \sum_p \tilde{I}^{pp}(k, p) G(p) \bar{\Delta}(p) G(-p), \quad (\text{C1})$$

where  $\tilde{I}^{pp}$  denotes the exact particle-particle irreducible four-point vertex. The diagrammatic expression is shown in Fig. 8(c).

Next, within the BS equation theory,  $\tilde{I}^{pp}$  is approximated as

$$\tilde{I}^{pp}(k, p) = \Gamma^{\text{SC}}(k, p), \quad (\text{C2})$$

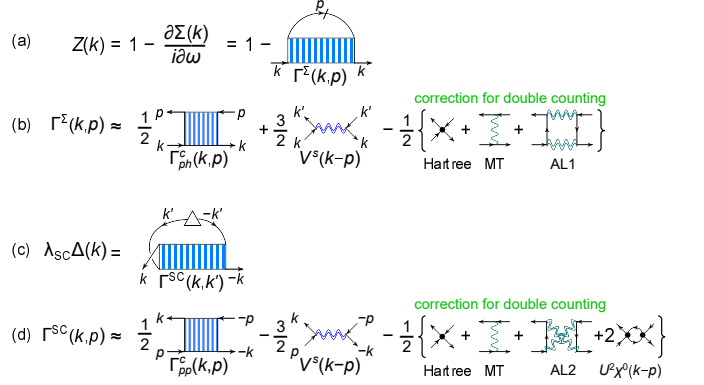


FIG. 8. (a) Diagrammatic expression of  $Z(k)$ . (b) Diagrammatic expression of  $\Gamma^\Sigma(k, p)$  used in the present numerical calculation. (c) Diagrammatic expression of the linearized gap equation. (d) Diagrammatic expression of  $\Gamma^{\text{SC}}(k, p)$  used in the present numerical calculation.

and

$$\Gamma^{\text{SC}}(k, p) = \frac{1}{2} \Gamma_{pp}^c(k, p) - \frac{3}{2} \Gamma_{pp}^s(k, p), \quad (\text{C3})$$

which is shown in Fig. 8(d). In Fig. 8(d), the double counting terms that should be subtracted are expressed.

Finally, in the present numerical calculation,

$$\lambda_{\text{SC}} \bar{\Delta}(k) = \frac{T}{N} \sum_p \Gamma^{\text{SC}}(k, p) G(p) \bar{\Delta}(p) G(-p). \quad (\text{C4})$$

Here,  $\Gamma^{\text{SC}}(k, p)$  is obtained by the lowest-Matsubara-frequency approximation:  $\Gamma_{pp}^c$  at  $|\epsilon_n| = \pi T$  is computed from the BS equation including vertex corrections, while other frequency components are taken from FLEX. Also,  $\Gamma_{pp}^s$  is taken from FLEX (i.e.,  $\Gamma_{pp}^s = V^s$ ). The correction terms are shown in Fig. 8(d). Numerically, we solve the linearized gap equation on the FSs [67].

## Appendix D: Supplementary analysis of charge-channel vertices

Figures 9(a) and 9(b) show  $I^c(\theta, \theta')$  for  $U = 4.29$ ,  $T = 0.01$ , and  $p = 0.2$ . It takes large positive values along the lines satisfying  $\theta = \theta' + \pi$  and  $\theta = -\theta'$ . This originates from the AL terms: in Eqs. (A12) and (A13), if the momentum dependence of  $W$  is neglected, the momentum summation of the product of internal Green's functions becomes large when  $\mathbf{k} = -\mathbf{k}$ . For small  $U$ , one has  $I^c \approx -U < 0$ . Therefore,  $I^c > 0$  is due to the vertex corrections.

Figure 9(c) shows  $\Gamma_{ph}^c$  for  $U = 4.0$ ,  $T = 0.01$ , and  $p = 0.2$ . Figure 9(d) shows  $\Gamma_{pp}^c$  for  $U = 4.0$ ,  $T = 0.01$ , and  $p = 0.2$ . Although the absolute values are smaller than those at  $U = 4.29$  shown in Figs. 3(a) and 3(b) in the main text, they exhibit very similar  $\theta, \theta'$  dependence.

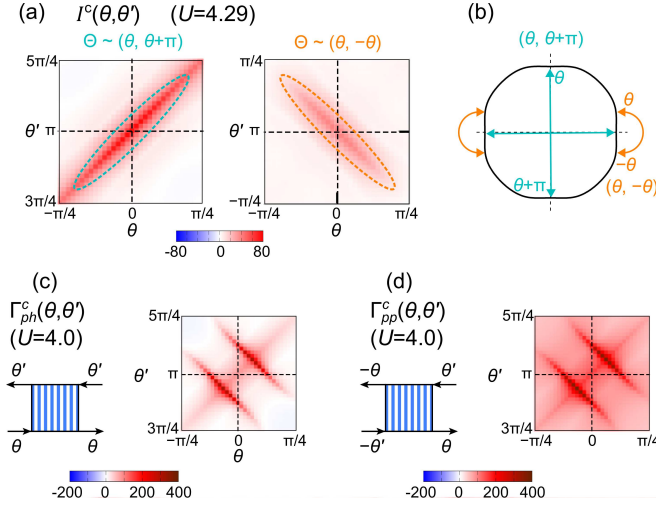


FIG. 9. (a)  $I^c = (I^c_{ph} + I^c_{pp})/2$  for  $U = 4.29$ ,  $T = 0.01$ , and  $p = 0.2$ . (b) Schematic illustration of the scattering process where  $I^c$  develops. (c)  $\Gamma^c_{ph}$  for  $U = 4.0$ . (d)  $\Gamma^c_{pp}$  for  $U = 4.0$ .

- 
- [1] G. Ghiringhelli, M. Le Tacon, M. Minola, S. Blanco-Canosa, C. Mazzoli, N. B. Brookes, G. M. De Luca, A. Frano, D. G. Hawthorn, F. He, T. Loew, M. Moretti Sala, D. C. Peets, M. Salluzzo, E. Schierle, R. Sutarto, G. A. Sawatzky, E. Weschke, B. Keimer, and L. Braicovich, Long-range incommensurate charge fluctuations in  $(Y,Nd)Ba_2Cu_3O_{6+x}$ , *Science* **337**, 821 (2012).
- [2] R. Comin, A. Frano, M. M. Yee, Y. Yoshida, H. Eisaki, E. Schierle, E. Weschke, R. Sutarto, F. He, A. Soumyanarayanan, Y. He, M. Le Tacon, I. S. Elfimov, J. E. Hoffman, G. A. Sawatzky, B. Keimer, and A. Damascelli, Charge order driven by Fermi-arc instability in  $Bi_2Sr_{2-x}La_xCuO_{6+\delta}$ , *Science* **343**, 390 (2014), epub 19 December 2013.
- [3] W. Tabis, Y. Li, M. L. Tacon, L. Braicovich, A. Kreyssig, M. Minola, G. Della, E. Weschke, M. J. Veit, M. Ramazanoglu, A. I. Goldman, T. Schmitt, G. Ghiringhelli, N. Barišić, M. K. Chan, C. J. Dorow, G. Yu, X. Zhao, B. Keimer, and M. Greven, Charge order and its connection with Fermi-liquid charge transport in a pristine high- $T_c$  cuprate, *Nature Communications* **5**, 5875 (2014).
- [4] J. Chang, E. Blackburn, O. Ivashko, A. T. Holmes, N. B. Christensen, M. Hücker, R. Liang, D. A. Bonn, W. N. Hardy, U. Rütt, M. V. Zimmermann, E. M. Forgan, and S. M. Hayden, Magnetic field controlled charge density wave coupling in underdoped  $YBa_2Cu_3O_{6+x}$ , *Nature Communications* **7**, 11494 (2016).
- [5] S. Gerber, H. Jang, H. Nojiri, S. Matsuzawa, H. Yasumura, D. A. Bonn, R. Liang, W. N. Hardy, Z. Islam, A. Mehta, S. Song, M. Sikorski, D. Stefanescu, Y. Feng, S. A. Kivelson, T. P. Devereaux, Z.-X. Shen, C.-C. Kao, W.-S. Lee, D. Zhu, and J.-S. Lee, Three-dimensional charge density wave order in  $YBa_2Cu_3O_{6.67}$  at high magnetic fields, *Science* **350**, 949 (2015).
- [6] H.-H. Kim, E. Lefrançois, K. Kummer, R. Fumagalli, N. B. Brookes, D. Betto, S. Nakata, M. Tortora, J. Porras, T. Loew, M. E. Barber, L. Braicovich, A. P. Mackenzie, C. W. Hicks, B. Keimer, M. Minola, and M. Le Tacon, Charge density waves in  $YBa_2Cu_3O_{6.67}$  probed by resonant x-ray scattering under uniaxial compression, *Phys. Rev. Lett.* **126**, 037002 (2021).
- [7] E. H. da Silva Neto, R. Comin, F. He, R. Sutarto, Y. Jiang, R. L. Greene, G. A. Sawatzky, and A. Damascelli, Charge ordering in the electron-doped superconductor  $Nd_{2-x}Ce_xCuO_4$ , *Science* **347**, 282 (2015).
- [8] Y. Y. Peng, R. Fumagalli, Y. Ding, M. Minola, S. Caprara, D. Betto, M. Bluschke, G. M. D. Luca, K. Kummer, E. Lefrançois, M. Salluzzo, H. Suzuki, M. L. Tacon, X. J. Zhou, N. B. Brookes, B. Keimer, L. Braicovich, M. Grilli, and G. Ghiringhelli, Re-entrant charge order in overdoped  $(Bi,Pb)_{2.12}Sr_{1.88}CuO_{6+\delta}$  outside the pseudogap regime, *Nature Materials* **17**, 697 (2018).
- [9] R. Arpaia, S. Caprara, R. Fumagalli, G. D. Vecchi, Y. Y. Peng, E. Andersson, D. Betto, G. M. D. Luca, N. B. Brookes, F. Lombardi, M. Salluzzo, L. Braicovich, C. D. Castro, M. Grilli, and G. Ghiringhelli, Dynamical charge density fluctuations pervading the phase diagram of a Cu-based high- $T_c$  superconductor, *Science* **365**, 906 (2019).
- [10] Y. Kohsaka, T. Hanaguri, M. Azuma, M. Takano, J. C. Davis, and H. Takagi, Visualization of the emergence of the pseudogap state and the evolution to superconductivity in a lightly hole-doped mott insulator, *Nature Physics* **8**, 534 (2012).
- [11] K. Fujita, M. H. Hamidian, S. D. Edkins, C. K. Kim, Y. Kohsaka, M. Azuma, M. Takano, H. Takagi, H. Eisaki, S. I. Uchida, A. Allais, M. J. Lawler, E. A. Kim, S. Sachdev, and J. C. S. Davis, Direct phase-sensitive identification of a  $d$ -form factor density wave in underdoped cuprates, *Proceedings of the National Academy of Sciences* **111**, E3026 (2014).
- [12] T. Wu, H. Mayaffre, S. Krämer, M. Horvatić, C. Berthier, W. N. Hardy, R. Liang, D. A. Bonn, and M.-H. Julien, Incipient charge order observed by NMR in the normal

- state of  $\text{YBa}_2\text{Cu}_3\text{O}_y$ , *Nature Communications* **6**, 6438 (2015).
- [13] S. Kawasaki, Z. Li, M. Kitahashi, C. T. Lin, P. L. Kuhns, A. P. Reyes, and G. qing Zheng, Charge-density-wave order takes over antiferromagnetism in  $\text{Bi}_2\text{Sr}_{2-x}\text{La}_x\text{CuO}_6$  superconductors, *Nature Communications* **8**, 1267 (2017).
- [14] I. Vinograd, R. Zhou, M. Hirata, T. Wu, H. Mayaffre, S. Krämer, R. Liang, W. N. Hardy, D. A. Bonn, and M.-H. Julien, Locally commensurate charge-density wave with three-unit-cell periodicity in  $\text{YBa}_2\text{Cu}_3\text{O}_y$ , *Nature Communications* **12**, 3274 (2021).
- [15] J.-H. Chu, J. G. Analytis, K. D. Greve, P. L. McMahon, Z. Islam, Y. Yamamoto, and I. R. Fisher, In-plane resistivity anisotropy in an underdoped iron arsenide superconductor, *Science* **329**, 824 (2010).
- [16] A. E. Böhrer and A. Kreisel, Nematicity, magnetism and superconductivity in FeSe, *Journal of Physics: Condensed Matter* **30**, 023001 (2017).
- [17] B. R. Ortiz, S. M. L. Teicher, Y. Hu, J. L. Zuo, P. M. Sarte, E. C. Schueller, A. M. M. Abeykoon, M. J. Krogstad, S. Rosenkranz, R. Osborn, R. Seshadri, L. Balents, J. He, and S. D. Wilson,  $\text{CsV}_3\text{Sb}_5$ : A  $\text{Z}_2$  topological kagome metal with a superconducting ground state, *Phys. Rev. Lett.* **125**, 247002 (2020).
- [18] H. Li, H. Zhao, B. R. Ortiz, T. Park, M. Ye, L. Balents, Z. Wang, S. D. Wilson, and I. Zeljkovic, Rotation symmetry breaking in the normal state of a kagome superconductor  $\text{KV}_3\text{Sb}_5$ , *Nature Physics* **18**, 265 (2022).
- [19] Y.-X. Jiang, J.-X. Yin, M. M. Denner, N. Shumiya, B. R. Ortiz, G. Xu, Z. Guguchia, J. He, M. S. Hossain, X. Liu, J. Ruff, L. Kautzsch, S. S. Zhang, G. Chang, I. Belopolski, Q. Zhang, T. A. Cochran, D. Multer, M. Litskevich, Z.-J. Cheng, X. P. Yang, Z. Wang, R. Thomale, T. Neupert, S. D. Wilson, and M. Z. Hasan, Unconventional chiral charge order in kagome superconductor  $\text{KV}_3\text{Sb}_5$ , *Nature Materials* **20**, 1353 (2021).
- [20] Y. Xing, S. Bae, E. Ritz, F. Yang, T. Birol, A. N. C. Salinas, B. R. Ortiz, S. D. Wilson, Z. Wang, R. M. Fernandes, and V. Madhavan, Optical manipulation of the charge-density-wave state in  $\text{RbV}_3\text{Sb}_5$ , *Nature* **631**, 60 (2024).
- [21] H. Deng, H. Qin, G. Liu, T. Yang, R. Fu, Z. Zhang, X. Wu, Z. Wang, Y. Shi, J. Liu, H. Liu, X.-Y. Yan, W. Song, X. Xu, Y. Zhao, M. Yi, G. Xu, H. Hohmann, S. C. Holbæk, M. Dürnagel, S. Zhou, G. Chang, Y. Yao, Q. Wang, Z. Guguchia, T. Neupert, R. Thomale, M. H. Fischer, and J.-X. Yin, Chiral kagome superconductivity modulations with residual Fermi arcs, *Nature* **632**, 775 (2024).
- [22] B. Keimer, S. A. Kivelson, M. R. Norman, S. Uchida, and J. Zaanen, From quantum matter to high-temperature superconductivity in copper oxides, *Nature* **518**, 179 (2015).
- [23] B. J. Ramshaw, S. E. Sebastian, R. D. McDonald, J. Day, B. S. Tan, Z. Zhu, J. B. Betts, R. Liang, D. A. Bonn, W. N. Hardy, and N. Harrison, Quasiparticle mass enhancement approaching optimal doping in a high- $T_c$  superconductor, *Science* **348**, 317 (2015).
- [24] J. Chang, N. Doiron-Leyraud, O. Cyr-Choinière, G. Grissonnanche, F. Laliberté, E. Hassinger, J.-P. Reid, R. Daou, S. Pyon, T. Takayama, H. Takagi, and L. Taillefer, Decrease of upper critical field with underdoping in cuprate superconductors, *Nature Physics* **8**, 751 (2012).
- [25] K. Mukasa, K. Ishida, S. Imajo, M. Qiu, M. Saito, K. Matsuura, Y. Sugimura, S. Liu, Y. Uezono, T. Otsuka, M. Čulo, S. Kasahara, Y. Matsuda, N. E. Hussey, T. Watanabe, K. Kindo, and T. Shibauchi, Enhanced superconducting pairing strength near a pure nematic quantum critical point, *Phys. Rev. X* **13**, 011032 (2023).
- [26] K. Y. Chen, N. N. Wang, Q. W. Yin, Y. H. Gu, K. Jiang, Z. J. Tu, C. S. Gong, Y. Uwatoko, J. P. Sun, H. C. Lei, J. P. Hu, and J.-G. Cheng, Double superconducting dome and triple enhancement of  $T_c$  in the kagome superconductor  $\text{csv}_3\text{sb}_5$  under high pressure, *Phys. Rev. Lett.* **126**, 247001 (2021).
- [27] T. Maier, M. Jarrell, T. Pruschke, and M. H. Hettler, Quantum cluster theories, *Rev. Mod. Phys.* **77**, 1027 (2005).
- [28] T. Schäfer, N. Wentzell, F. Šimkovic, Y.-Y. He, C. Hille, M. Klett, C. J. Eckhardt, B. Arzhang, V. Harkov, F. m. c.-M. Le Régent, A. Kirsch, Y. Wang, A. J. Kim, E. Kozik, E. A. Stepanov, A. Kauch, S. Andergassen, P. Hansmann, D. Rohe, Y. M. Vilk, J. P. F. LeBlanc, S. Zhang, A.-M. S. Tremblay, M. Ferrero, O. Parcollet, and A. Georges, Tracking the footprints of spin fluctuations: A multimethod, multimessenger study of the two-dimensional hubbard model, *Phys. Rev. X* **11**, 011058 (2021).
- [29] H. Yokoyama and H. Shiba, Variational Monte-Carlo studies of Hubbard model. i, *J. Phys. Soc. Jpn.* **56**, 1490 (1987).
- [30] S. Sorella, Generalized lanczos algorithm for variational quantum monte carlo, *Phys. Rev. B* **64**, 024512 (2001).
- [31] S. Karakuzu, A. T. Ly, P. Mai, J. Neuhaus, T. A. Maier, and S. Johnston, Stripe correlations in the two-dimensional Hubbard-Holstein model, *Communications Physics* **5**, 311 (2022).
- [32] S. R. White, Density matrix formulation for quantum renormalization groups, *Phys. Rev. Lett.* **69**, 2863 (1992).
- [33] J. P. F. LeBlanc, A. E. Antipov, F. Becca, I. W. Bulik, G. K.-L. Chan, C.-M. Chung, Y. Deng, M. Ferrero, T. M. Henderson, C. A. Jiménez-Hoyos, E. Kozik, X.-W. Liu, A. J. Millis, N. V. Prokof'ev, M. Qin, G. E. Scuseria, H. Shi, B. V. Svistunov, L. F. Tocchio, I. S. Tupitsyn, S. R. White, S. Zhang, B.-X. Zheng, Z. Zhu, and E. Gull, Solutions of the two-dimensional hubbard model: Benchmarks and results from a wide range of numerical algorithms, *Phys. Rev. X* **5**, 041041 (2015).
- [34] E. Stoudenmire and S. R. White, Studying two-dimensional systems with the density matrix renormalization group, *Annual Review of Condensed Matter Physics* **3**, 111 (2012).
- [35] M. Salmhofer and C. Honerkamp, Fermionic renormalization group flows: Technique and theory, *Progress of Theoretical Physics* **105**, 1 (2001).
- [36] W. Metzner, M. Salmhofer, C. Honerkamp, V. Meden, and K. Schönhammer, Functional renormalization group approach to correlated fermion systems, *Rev. Mod. Phys.* **84**, 299 (2012).
- [37] A. T. Zheleznyak, V. M. Yakovenko, and I. E. Dzyaloshinskii, Parquet solution for a flat fermi surface, *Phys. Rev. B* **55**, 3200 (1997).
- [38] R. Tazai, Y. Yamakawa, S. Onari, and H. Kontani, Mechanism of exotic density-wave and beyond-migdal unconventional superconductivity in kagome metal  $\text{AV}_3\text{Sb}_5$  ( $A = \text{K, Rb, Cs}$ ), *Science Advances* **8**, eabl4108 (2022).
- [39] R. Tazai, Y. Yamakawa, M. Tsuchiizu, and H. Kon-

- tani, Functional renormalization group study of orbital fluctuation mediated superconductivity: Impact of the electron-boson coupling vertex corrections, *Phys. Rev. B* **94**, 115155 (2016).
- [40] R. Tazai, Y. Yamakawa, and H. Kontani, Emergence of charge loop current in the geometrically frustrated hubbard model: A functional renormalization group study, *Phys. Rev. B* **103**, L161112 (2021).
- [41] M. Tsuchiizu, Y. Ohno, S. Onari, and H. Kontani, Orbital nematic instability in the two-orbital Hubbard model: Renormalization-group + constrained rpa analysis, *Phys. Rev. Lett.* **111**, 057003 (2013).
- [42] M. Tsuchiizu, K. Kawaguchi, Y. Yamakawa, and H. Kontani, Multistage electronic nematic transitions in cuprate superconductors: A functional-renormalization-group analysis, *Phys. Rev. B* **97**, 165131 (2018).
- [43] A. V. Chubukov, M. Khodas, and R. M. Fernandes, Magnetism, superconductivity, and spontaneous orbital order in iron-based superconductors: Which comes first and why?, *Phys. Rev. X* **6**, 041045 (2016).
- [44] S. Onari and H. Kontani, Self-consistent vertex correction analysis for iron-based superconductors: Mechanism of coulomb interaction-driven orbital fluctuations, *Phys. Rev. Lett.* **109**, 137001 (2012).
- [45] Y. Yamakawa, S. Onari, and H. Kontani, Nematicity and magnetism in fese and other families of Fe-based superconductors, *Phys. Rev. X* **6**, 021032 (2016).
- [46] Y. Yamakawa and H. Kontani, Spin-fluctuation-driven nematic charge-density wave in cuprate superconductors: Impact of aslamazov-larkin vertex corrections, *Phys. Rev. Lett.* **114**, 257001 (2015).
- [47] K. Kawaguchi, Y. Yamakawa, M. Tsuchiizu, and H. Kontani, Competing unconventional charge-density-wave states in cuprate superconductors: Spin-fluctuation-driven mechanism, *J. Phys. Soc. Jpn.* **86**, 063707 (2017).
- [48] H. Kontani, R. Tazai, Y. Yamakawa, and S. Onari, Unconventional density waves and superconductivities in Fe-based superconductors and other strongly correlated electron systems, *Advances in Physics* **70**, 355 (2021).
- [49] G. Baym and L. P. Kadanoff, Conservation laws and correlation functions, *Phys. Rev.* **124**, 287 (1961).
- [50] R. Tazai, S. Matsubara, Y. Yamakawa, S. Onari, and H. Kontani, Rigorous formalism for unconventional symmetry breaking in fermi liquid theory and its application to nematicity in fese, *Phys. Rev. B* **107**, 035137 (2023).
- [51] J. A. Hertz, Quantum critical phenomena, *Phys. Rev. B* **14**, 1165 (1976).
- [52] A. J. Millis, Effect of a nonzero temperature on quantum critical points in itinerant fermion systems, *Phys. Rev. B* **48**, 7183 (1993).
- [53] N. E. Bickers, D. J. Scalapino, and S. R. White, Conserving approximations for strongly correlated electron systems: Bethe-salpeter equation and dynamics for the two-dimensional hubbard model, *Phys. Rev. Lett.* **62**, 961 (1989).
- [54] N. E. Bickers and S. R. White, Conserving approximations for strongly fluctuating electron systems. ii. numerical results and parquet extension, *Phys. Rev. B* **43**, 8044 (1991).
- [55] A. A. Abrikosov, L. P. Gorkov, and I. E. Dzyaloshinski, *Methods of Quantum Field Theory in Statistical Physics* (Dover, New York, 1963).
- [56] T. Moriya and K. Ueda, Spin fluctuations and high temperature superconductivity, *Advances in Physics* **49**, 555 (2000).
- [57] R. Tazai, Y. Yamakawa, M. Tsuchiizu, and H. Kontani, Plain s-wave superconductivity near magnetic criticality: Enhancement of attractive electron-boson coupling vertex corrections, *J. Phys. Soc. Jpn.* **86**, 073703 (2017).
- [58] R. Tazai and H. Kontani, Multipole fluctuation theory for heavy fermion systems: Application to multipole orders in  $\text{CeB}_6$ , *Phys. Rev. B* **100**, 241103 (2019).
- [59] Y. Yamakawa and H. Kontani, Superconductivity without a hole pocket in electron-doped FeSe: Analysis beyond the migdal-eliasberg formalism, *Phys. Rev. B* **96**, 045130 (2017).
- [60] S. Onari, Y. Yamakawa, and H. Kontani, High- $T_c$  superconductivity near the anion height instability in Fe-based superconductors: Analysis of  $\text{LaFeAsO}_{1-x}\text{H}_x$ , *Phys. Rev. Lett.* **112**, 187001 (2014).
- [61] H. Kontani, K. Kanki, and K. Ueda, Hall effect and resistivity in high- $T_c$  superconductors: The conserving approximation, *Phys. Rev. B* **59**, 14723 (1999).
- [62] T. Moriya, *Spin Fluctuations in Itinerant Electron Magnetism*, Springer Series in Solid-State Sciences, Vol. 56 (Springer, Berlin Heidelberg, 1985).
- [63] Y. Yamakawa, S. Onari, and H. Kontani, Doping effects on electronic states in electron-doped FeSe: Impact of self-energy and vertex corrections, *Phys. Rev. B* **102**, 081108(R) (2020).
- [64] Y. Yamakawa and H. Kontani, Nematicity, magnetism, and superconductivity in FeSe under pressure: Unified explanation based on the self-consistent vertex correction theory, *Phys. Rev. B* **96**, 144509 (2017).
- [65] M. A. Hossain, J. D. F. Mottershead, D. Fournier, A. Bostwick, J. L. McChesney, E. Rotenberg, R. Liang, W. N. Hardy, G. A. Sawatzky, I. S. Elfimov, D. A. Bonn, and A. Damascelli, In situ doping control of the surface of high-temperature superconductors, *Nature Physics* **4**, 527 (2008).
- [66] R. Tazai and H. Kontani, Fully gapped s-wave superconductivity enhanced by magnetic criticality in heavy-fermion systems, *Phys. Rev. B* **98**, 205107 (2018).
- [67] D. Inoue, Y. Yamakawa, S. Onari, and H. Kontani, Unified mechanism of charge-density-wave and high- $T_c$  superconductivity protected from oxygen vacancies in bilayer nickelates (2025), [arXiv:2503.12925 \[cond-mat.supr-con\]](https://arxiv.org/abs/2503.12925).
- [68] H. Kontani, Y. Yamakawa, R. Tazai, and S. Onari, Odd-parity spin-loop-current order mediated by transverse spin fluctuations in cuprates and related electron systems, *Phys. Rev. Res.* **3**, 013127 (2021).